Multiscale Simulation Using Generalized Interpolation Material Point (GIMP) Method and Molecular Dynamics (MD)[1]

J. Ma[2], H. Lu[2], B. Wang[2], R. Hornung[3], A. Wissink[3], and R. Komanduri[2,*]

Abstract: A new method for multiscale simulation bridging two scales, namely, the continuum scale using the generalized interpolation material point (GIMP) method and the atomistic scale using the molecular dynamics (MD), is presented and verified in 2D. The atomistic strain from the molecular dynamics simulation is determined through interpolation of the displacement field into an Eulerian background grid using the same generalized interpolation functions as that in the GIMP method. The atomistic strain is consistent with that determined from the virial theorem for interior points but provides more accurate values at the boundary of the MD region and in the transition region between MD-GIMP. A material point in the continuum is split into smaller material points using multi-level refinement until it has nearly reached the atom size to couple with atoms in the MD region. Consequently, coupling between GIMP and MD is achieved by using compatible deformation, force, and energy fields in the transition region between GIMP and MD. The coupling algorithm is implemented in the Structural Adaptive Mesh Refinement Application Infrastructure (SAMRAI) for parallel processing. Both mode I and mode II crack problems are simulated using the coupling algorithm. The stress field near the crack tip was verified by comparing the results from the coupled simulations with purely GIMP simulations of the same model. Coupled simulation results were also compared with pure MD simulation results. In both cases, a very good agreement was obtained.

keyword: Incremental atomic strain, Multiscale simulation, GIMP, MD, Coupling, SAMRAI, Crack, Friction.

1 Introduction

Simulations at the continuum and atomistic levels are often used to determine the material deformation and failure at their respective length scales. The atomistic simulations are usually performed at very small length scales (from nanometer to micrometer scales) and time scales (a microsecond or less) whereas continuum simulations are performed at larger temporal and spatial scales. While an atomistic scale simulation can reveal the fundamental aspects of deformation and failure behavior, it cannot be scaled up for larger length scales due to limitation in computing power. However, for nanoindentation and crack propagation problems, a combined atomistic and continuum simulation may provide as much information as a purely atomistic simulation would provide. This is especially so when MD simulations are used for regions encompassing high stress gradient zones, such as the crack propagation zone (Kohlhoff, Gumbsch and Fischmeister (1991)) and the workpiece just underneath the indenter as in nanoindentation (Shilkrot, Miller and Curtin (2002)) and a continuum region is used for rest of the material.

Several techniques have been proposed for simulations bridging two or more scales (Kohlhoff, Gumbsch and Fischmeister (1991); Shilkrot, Miller and Curtin (2002); Curtin and Miller (2003); Shiari, Miller and Curtin (2005); Raffi-Tabar, Hua and Cross (1998)). A transition region, or handshake region, overlapped by the outer boundary of the atomistic region and the inner boundary of the continuum region, is usually used to transfer the physical quantities (Kohlhoff, Gumbsch and Fischmeister (1991); Shilkrot, Miller and Curtin (2002); Curtin and Miller (2003)). In multiscale simulation, the finite element method (FEM) is often used at the continuum level. However, waves with wavelengths larger than the element size can be transmitted from the MD region into the continuum region, and waves with wave-

[2] School of Mechanical and Aerospace Engineering, Oklahoma State University, Stillwater, OK 74078. *Correspondence author, Tel: 405-744-5900; Fax: 405-744-7873; e-mail: ranga@ceat.okstate.edu
[3] Center for Applied Scientific Computing, Lawrence Livermore National Laboratory, Livermore, CA 94551.

length smaller than the element size get reflected artificially (Raffi-Tabar, Hua and Cross (1998)). Efforts were made to minimize the wave reflection while enforcing the displacement and force continuity, as well as energy conservation in the handshake region. An intermediate scale, namely, the mesoscale simulation was also used in bridging the continuum and atomistic simulations (Raffi-Tabar, Hua and Cross (1998)). Recently, nonlinear deformation has been considered in coupling to capture more physical phenomenon. The coupled atomistic/continuum discrete dislocation (CADD) method has demonstrated superior capability in detecting dislocations from MD simulation and passing them to the continuum region, as well as handling explicit material defects and inclusions (Shiari, Miller and Curtin (2005)). For 2D simulations, the dislocations generated in the atomistic region can propagate into the continuum region by defining continuum elements with slip planes in front of the transition region to detect dislocations (Shilkrot, Miller and Curtin (2002); Curtin and Miller (2003)).

Other simulation techniques, such as the meshless local Petrov-Galerkin (MLPG) method (Shen and Atluri (2005)), Green's function method (Cai, Koning, Bulatov and Yip (2000)), and coarse-grained molecular dynamics (Rudd, Broughton (1998)) are also used at the continuum level. These techniques show advantages in heat transfer, stress compatibility, and minimizing wave reflection for the coupling between atomistic and continuum levels. Mesh distortion associated with FEM is an issue for large nonlinear deformations and dislocations. Recently, the material point method (MPM) (Sulsky, Zhou and Schreyer (1995); Sulsky and Schreyer (1996)) was introduced for dynamic simulations and the general interpolation material point (GIMP) method (Bardenhagen and Kober (2004)) was presented with improved simulation stability. The MPM and GIMP use material points to represent a material continuum and utilizes both the Lagrangian description for material points carrying physical quantities and the Eulerian description for convection of physical variables and solution of field equations. Since the GIMP/MPM methods do not use a fixed body mesh so that mesh entanglement associated with highly nonlinear deformations can be prevented. GIMP and MPM have been used in the computation of stresses and strains in metal forming, dynamic fracture (Guo and Nairn (2004)), and impact problems (Sulsky and Shreyer (1996)). Recently, GIMP has been

successfully implemented for 2D simulations covering length scales from nanometers to millimeters (Ma, Wang, Lu, Roy, Hornung, Wissink and Komanduri (2005)) using multi-level mesh refinement with parallel computing in the Structured Adaptive Mesh Refinement Infrastructure (SAMRAI) (Hornung and Kohn (2002)) framework. The GIMP refinement technique proposed here has made it possible for coupling with MD so that the advantages of GIMP/MPM methods can be fully carried over to multiscale simulations. This paper will describe the GIMP/MD coupling techniques, and demonstrate it in the mode I and mode II crack propagation problems.

One aspect of the problems associated with coupling is the conversion of physical quantities computed from MD region to continuum region, and vice versa. MD simulation gives atom positions, velocities, etc. The stresses and strains defined in a material continuum can be computed from MD simulation using various approaches (Gao, Huang and Abraham (2001); Buehler, Abraham and Gao (2003); Zimmermann (1999); Horstemeyer and Baskes (2000)). The most effective standard approach is based on the virial theorem (Marc and McMillan (1985); Zimmermann, Webb, Hoyt, Jones, Klein, Bammann (2004)). However, this approach cannot be used to calculate the strain at the boundary of the MD region. Some new approaches have been developed to calculate the atomic stress more accurately. For example, Zhou and McDowell (2004) defined an equivalent continuum for the atomistic system with conserved momenta, work rates, and mass. The atomic stresses are then calculated from the internal forces and lattice constants. Hardy, Root and Swanson (2002) computed the atomic stresses from the contribution of nearby atoms with spatial averaging formulation using a finite-valued and finite-ranged localization function (Zimmermann, Webb, Hoyt, Jones, Klein and Bammann (2004)).

The atomistic strain measures the deformation of the atomic lattice. It is also used in combined atomistic and continuum studies of material behavior. Buehler, Gao and Huang (2004) investigated the stress and strain fields near the crack tip in MD simulations and revealed that continuum mechanics can be used at nanoscale. In another study, Bueher, Abraham and Gao (2003) showed that the hyperelasticity is crucial for dynamic brittle fracture and when the hyperelastic zone approaches the energy length scale, which is defined as a function of the modulus and applied stress, the energy transport process

is dominated by hyperelasticity in a harmonic solid with a mode I crack.

This paper presents a method for coupling MD with GIMP simulations in 2D. A new formulation to compute the atomistic strain rate and strain increment is developed by computing the velocity gradient based on the interpolation of the velocity field on a background grid. Based on the atomic strain computation, an equivalent continuum can be defined for the atomic region for the purpose of coupling MD with continuum computations using the GIMP method. The coupled GIMP and MD simulations use the same background mesh. The coupling scheme is based on the atomistic strain, stress, and deformation. The heat conduction is neglected in current simulation, but it can be included in the coupling algorithm with further work. Both mode I and mode II crack propagation problems are simulated to demonstrate the coupling approaches. The coupled simulation results are compared with purely GIMP simulations, and pure MD simulation for verification.
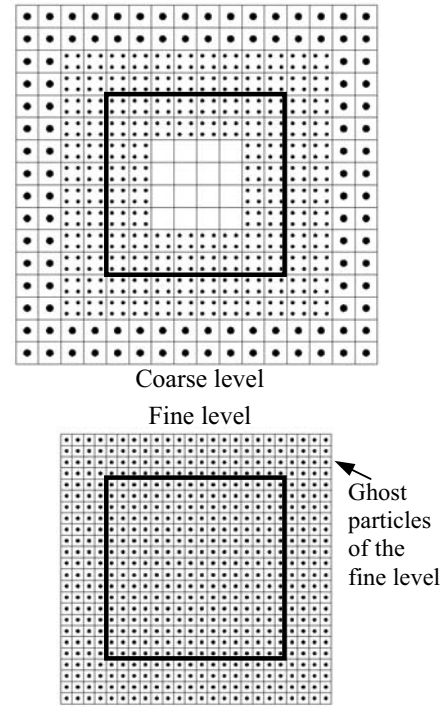
2 GIMP and Refinement

In the generalized interpolation material point method (GIMP) (Bardenhagen and Kober (2004)), a continuum is discretized into a collection of material points. Each material point carries all the physical variables for a fully defined problem in solid mechanics, such as the position, mass, velocity, stress and strain, etc. Each material point deforms to represent the motion of the continuum while the mass at each material point remains constant. For a dynamic problem, using the variational principle, the balance of linear momentum is represented by

$$\int_\Omega \rho \mathbf{a} \cdot \delta \mathbf{v} dx + \int \boldsymbol{\sigma} : \nabla \delta \mathbf{v} dx = \int_\Omega \mathbf{b} \cdot \delta \mathbf{v} dx + \int_{\partial \Omega} \mathbf{c} \cdot \delta \mathbf{v} dx \quad (1)$$

where ρ is the mass density, $\mathbf{a}$ is the acceleration field, $\mathbf{b}$ is the body force density, $\boldsymbol{\sigma}$ is the Cauchy stress tensor, $\delta \mathbf{v}$ is an arbitrary admissible velocity field and Ω is a region in the current configuration (Bardenhagena and Kober (2004)). To solve this equation, a background grid is introduced for interpolation between the material points and the nodes on the background grid using a weighting function. Hence, Eq. (1) can be discretized and the equation of motion is eventually solved at each node,

$$\dot{\mathbf{p}}_i = \mathbf{f}_i^{int} + \mathbf{f}_i^b + \mathbf{f}_i^{ext}, \quad (2)$$

Coarse level

Fine level

Ghost particles of the fine level

Figure 1 : Two neighboring coarse and fine grid levels in 2D GIMP computations representation

where the nodal momentum, internal force and body force are obtained by summing the contributions from nearby material points p to node i as $\dot{\mathbf{p}}_i = \sum_p \overline{S}_{ip} \dot{\mathbf{p}}_p$, $\mathbf{f}_i^{int} = -\sum_p \boldsymbol{\sigma}_p \cdot \overline{\nabla S}_{ip} V_p$ and $\mathbf{f}_i^b = \sum_p m_p \mathbf{b} \overline{S}_{ip}$, respectively. m_p and V_p are the particle mass and volume, respectively. The external force is given by $\mathbf{f}_i^{ext} = \int_{\partial \Omega_c} \mathbf{c} S_i(\mathbf{x}) dS$, where $\mathbf{c}$ is the surface traction. $S_i(\mathbf{x})$ and $\overline{S}_{ip}$ are the grid interpolation function and the weight, respectively and their definitions will be given in section 3.2. Finally, the position, strain, and stress of the material points can be updated using the interpolation from surrounding nodes.

For GIMP simulations, finer computational mesh and smaller time step should be used to maintain accuracy in areas with high stress gradient. Both spatial and temporal refinements have been introduced in a multilevel refinement algorithm (Ma, Wang, Lu, Roy, Hornung, Wissink, and Komanduri (2005)) in which the computational domain consists of a hierarchy of nested grid levels with increasing refinement. Each finer level covers part of the next coarse level and each level is computed separately with its own time increment. Smaller time increments

are used for finer levels and the communication between two grid levels are performed when these two levels are synchronized. Figure 1 shows two neighboring coarse and fine grid levels in 2D GIMP computations with a refinement ratio of two. The thick line represents the physical boundary of the fine level with four layers of ghost cells. Initially, four material points are assigned to each cell at the fine level. At the coarse level, the portion overlapped by the fine level is assigned 4 material points per cell. Hence, these material points have the same size and initial positions as those at the fine level. The rest of the coarse level is assigned one material points per cell. Two data exchange processes, i.e., refinement and coarsening are used in the communication. The refinement process passes information from a coarser level to its next finer level, while the coarsening process passes information from a finer level to its next coarse level. In the refinement process, physical variables at the fine material points inside the thick lines are copied directly to replace the material points in the coarser level. In the coarsening process, the physical variables at coarse material points are copied to the ghost cells of the next finer level.

Using SAMRAI, each grid level can be divided into multiple patches for parallel processing. Each patch is rectangular and is assigned to a processor. The patches are overlapped by ghost cells for communication. The parallel processing scheme will be discussed in more detail in section 4.2.

3   MD Simulation and Atomistic Strain

Molecular dynamics (MD) simulations compute the motion of the atoms by integrating the equations of motion given by Newton's second law. In general, short range interaction among atoms within the cutoff radius is governed by an atomic potential function. With the rapid increase of computing power, MD simulation is becoming a powerful tool in simulation of material behavior. The MD code used in this paper is the LAMMPS code (Plimpton (1995)) developed at the Sandia National Laboratories.

To couple MD with a continuum simulation, using the GIMP method, we need to pass MD results to the continuum simulation. For this purpose, variables in MD must be consistent with those in the GIMP simulation. The most critical issue is passing the atom velocities and deformations to the continuum region. This involves the computation of continuum strain fields based on the discrete atom deformations.

$$B_{ij}^a = \frac{1}{\lambda} \sum_{b \neq a}^{N} \frac{\Delta x_i^{ab} \Delta x_j^{ab}}{R_{ab}^2} \tag{3}$$

where $\Delta x_i^{ab} = x_i^a - x_i^b$, $\Delta x_j^{ab} = x_j^a - x_j^b$, R_{ab} is the undeformed distance between atoms a and b, and N is usually limited to the nearest neighbors. λ is a factor depending on the lattice structure. For example, $\lambda = 3$ for the 2D triangular lattice if the six nearest neighboring atoms are considered only (Zimmermann (1999)). Therefore, the components of the Eulerian strain tensor for atom a are found as

$$\varepsilon_{ij}^a = \frac{1}{2}(\delta_{ij} - [B_{ij}^a]^{-1}) \tag{4}$$

where δ_{ij} is the Kronecker delta. The virial strain is meaningful instantaneously in time and space. However, at locations where the nearest neighbor list does not exist or cannot be determined, such as at the external boundary, crack surfaces and interfaces, Eq. (3) is invalid. To resolve this problem, we propose an alternative approach as described in the next section to calculate the atomistic strain based on the strain rate.

3.1   Incremental atomic strain

To construct the deformation field from the MD simulation, the GIMP Eulerian background grid is utilized. All the quantities defined at atoms, such as the mass, velocity, and forces can be projected to the background nodes through interpolation. While the nodal positions are fixed in space, the nodal quantities can vary with time. The velocity of atom a inside the grid is

$$\mathbf{v}(\mathbf{x}_a, t) = \sum_{i=1}^{n} \overline{S}_{ia}(\mathbf{x}_a) \mathbf{V}_i(t), \tag{5}$$

where n is the number of nodes and $\overline{S}_{ia}(\mathbf{x})$ is the interpolation function between node i and atom a. By definition, the infinitesimal strain tensor of atom a is then

$$\boldsymbol{\varepsilon}(\mathbf{x}_a, t) = \frac{1}{2}\{\nabla \mathbf{u}(\mathbf{x}_a, t) + [\nabla \mathbf{u}(\mathbf{x}_a, t)]^T\}, \tag{6}$$

where $\mathbf{u}(\mathbf{x}_a, t)$ is the displacement field. The strain rate is given by

$$\dot{\boldsymbol{\varepsilon}}(\mathbf{x}_a, t) = \frac{1}{2}\{\nabla \mathbf{v}(\mathbf{x}_a, t) + [\nabla \mathbf{v}(\mathbf{x}_a, t)]^T\}. \tag{7}$$

The velocity gradient at atom a can be expressed as $\nabla \mathbf{v}(\mathbf{x}_a, t) = \sum_{a=1}^{n} \nabla \overline{S}_{ia}(\mathbf{x}_a) \mathbf{V}_i(t)$. Using the backward Euler time integration scheme, we calculate the strain at atom a for the next time step through

$$\boldsymbol{\varepsilon}_a^{t+\Delta t} = \boldsymbol{\varepsilon}_a^t + \dot{\boldsymbol{\varepsilon}}_a^{t+\Delta t} \Delta t, \tag{8}$$

where $\dot{\boldsymbol{\varepsilon}}_a^{t+\Delta t} = \frac{1}{2} \sum_{i=1}^{n} (\nabla \overline{S}_{ia} \mathbf{V}_i^{t+\Delta t} + \mathbf{V}_i^{t+\Delta t} \nabla \overline{S}_{ia})$.

The nodal mass, force, and momentum are computed from neighboring atoms as $M_i^t = \sum_{a=1}^{n} \overline{S}_{ia} m_a^t$, $\mathbf{F}_i^t = \sum_{a=1}^{n} \overline{S}_{ia} \mathbf{f}_a^t$, $\mathbf{P}_i^t = \sum_{a=1}^{n} \overline{S}_{ia}(m_a^{t+\Delta t} \mathbf{v}_a^{t+\Delta t})$, respectively. The updated nodal momentum and velocity are $\mathbf{P}_i^{t+\Delta t} = \mathbf{P}_i^t + \mathbf{F}_i^t \Delta t$ and $\mathbf{V}_i^{t+\Delta t} = \mathbf{P}_i^{t+\Delta t} / M_i^t$.

3.2 Interpolation function

To ensure conservation of mass, momentum, and energy between the nodes and the atoms, the interpolation function should satisfy partition of unity. The interpolation function $\overline{S}_{ia}(\mathbf{x})$ can be chosen to be the isoparametric shape functions used in finite element analysis. However, the generalized interpolation functions with C^1 continuity in GIMP has shown better simulation stability when an Eulerian grid is used (Bardenhagen and Kober (2004); Ma, Wang, Lu, Roy, Hornung, Wissink and Komanduri (2005) and it is used to compute the atomic strain in this investigation.

The generalized interpolation function introduced by Bardenhagen and Kober (2004) consists of two functions, the nodal shape function and the particle characteristic function. Both the nodal shape function and the material point characteristic function can be extended to 3D. In three dimensional situations, the nodal shape function for node i is

$$S_i(\mathbf{x}) = S_i^x(x) S_i^y(y) S_i^z(z), \tag{9}$$

and the particle characteristic function for a brick particle p is

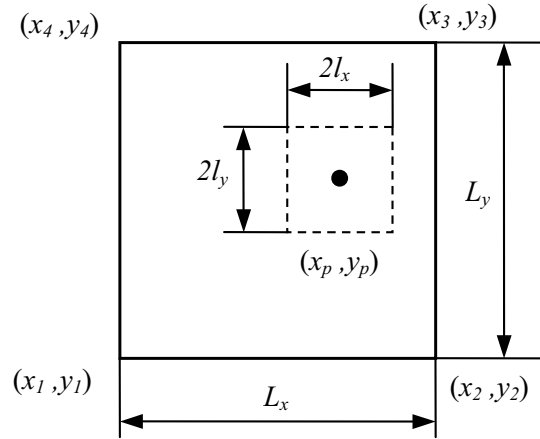$$\chi_p(\mathbf{x}) = \chi_p^x(x) \chi_p^y(y) \chi_p^z(z), \tag{10}$$

where

$$S_i^x(x) = \begin{cases} 0 & x - x_i \leq -L_x \\ 1 + (x - x_i)/L_x & -L_x \leq x - x_i \leq 0 \\ 1 - (x - x_i)/L_x & 0 \leq x - x_i \leq L_x \\ 0 & L_x \leq x - x_i \end{cases}, \tag{11}$$

and

$$\chi_p^x(x) = H[x - (x_p - l_x)] - H[x - (x_p + l_x)], \tag{12}$$

where $H(x)$ is the Heaviside step function.

**Figure 2** : 2D representation of a particle and a grid cell

Figure 2 shows a rectangular grid cell with a particle in it. The particle position is taken at the center of the particle. It may be noted that the grid associated with the generalized interpolation function is a structured grid, which is convenient to construct and process.

Both the nodal shape function and the particle characteristic function are a partition of unity, i.e., $\sum_p \chi_p(\mathbf{x}) = 1$ and $\sum_i S_i(\mathbf{x}) = 1$. The generalized interpolation function is a volume averaged weighting function between node i and material points p given by

$$\overline{S}_{ip} = \frac{1}{V_p} \int_{\Omega \cap \Omega_p} \chi_p(\mathbf{x}) S_i(\mathbf{x}) d\mathbf{x}, \tag{13}$$

where Ω is the entire computational region, Ω_p is the space occupied by particle p, and V_p is the current particle volume.

The atoms are generally considered as spherical in shape. The characteristic function of a sphere can also be found. However, to simplify the computation of the interpolation function and its gradient, we consider that the atoms are cubic in shape with the same volume of a spherical atom for the purpose of coupling. We also assume that the shape and orientation of the atoms do not change in
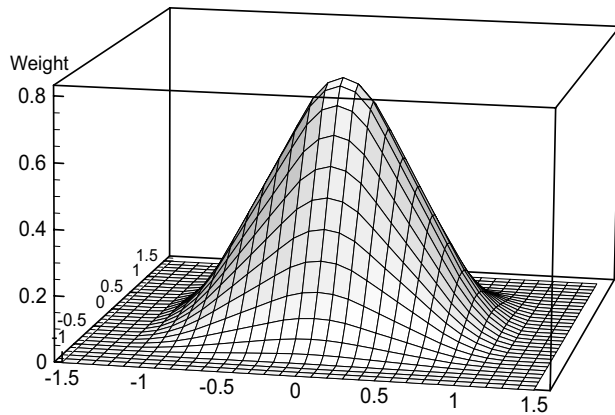
Figure 3 : The generalized interpolation function in 2D

the simulation. Consequently, Eq. (13) is simplified as

$$\overline{S}_{ip} = \frac{1}{8l_x l_y l_z} \int\limits_{x_p-l_x}^{x_p+l_x} S_i^x(x)dx \int\limits_{y_p-l_y}^{y_p+l_y} S_i^y(y)dy \int\limits_{z_p-l_z}^{z_p+l_z} S_i^z(z)dz. \quad (14)$$

The final expression of the interpolation function and its gradient can be found in Bardenhagen and Kober (2004). The interpolation function is plotted in Figure 3. The vertical axis is the interpolation function and horizontal plane is the particle position. The node is at (0, 0). The cell size is 1×1 and the particle size is 0.5×0.5. The interpolation function is C^1 continuous. We note that the sum of all the interpolation weights between an atom and its neighboring nodes is one.

3.3 Numerical verification

Several MD simulations are performed to calculate the atomistic strain in 2D. In these simulations, the atomic potential chosen is the Lennard-Jones potential given by

$$U(r) = 4\varepsilon_0 \left(\frac{\sigma^{12}}{r^{12}} - \frac{\sigma^6}{r^6} \right) \quad (15)$$

with $\varepsilon_0 = 1.0$ and $\sigma = 1$. The mass of each atom m_a is assumed to be 1. Dimensionless MD units are used in this study (see, Allen and Tildesley (1989)) and therefore, the units for time, velocity and stress/pressure are $\sigma\sqrt{m_a/\varepsilon_0}$, $\sqrt{\varepsilon_0/m_a}$ and ε_0/σ^3, respectively. The potential in Eq. (15) gives the longitudinal wave speed $c_l = 8.99$, the shear wave speed $c_s = 5.19$, and the Rayleigh wave speed $c_R = 4.80$. A 2D triangular lattice is used
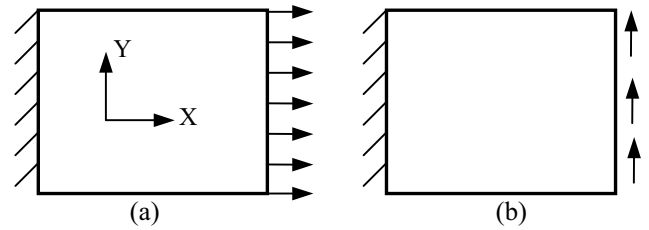

Figure 4 : Two examples to calculate the atomistic strains (a) Tension and (b) Shear

in the simulations. The model has 40 lattices in the X-direction and 20 lattices in the Y-direction. The size of the model is 44×39 and the cut off radius is 2.5. The atom is assumed to be cubic with a volume of unity.

The first simulation is simple tension, as shown in Figure 4 (a). The model is constrained in the X-direction on the left while a constant velocity is applied on two layers of lattices on the right. The strain histories of the atom initially at (24.5, 11.2) calculated using the virial formula and the new incremental approach are plotted in Figure 5 (a). It is seen that in general the strains calculated from different methods agree reasonably well. The virial strain shows more oscillations than the incremental strain. It may be noted that the interpolation between the nodes and the atoms is also a spatial averaging process. Two cell sizes, 2 and 2.5 are used in the background grid to investigate the effect of cell size. It can be seen that oscillations in the strain values are smaller when the cell size is bigger and vice versa because the nodal quantities are interpolated from a bigger number of atoms. A large content of noise, as a result of random thermal vibration of the atoms, has been suppressed due to averaging over a number of atoms. For comparison, the strain from continuum simulation (assuming the model material to be homogeneous, isotropic, and linearly elastic) using the finite element method is also plotted. It can be seen that all simulations show that the strain first increases at time between t = 2.5 and 3. The calculated rise time is t = 2.8 based on the longitudinal stress wave speed.

The second simulation is a shearing problem, as shown in Figure 4 (b). Constant upward velocity is applied on the two lattices on the right. The resulting shear strain at location (24.5, 11.2) is plotted in Figure 5 (b) from these simulations. The virial strain again shows largest variation while the strain computed from the incremental strain approach defined in this work shows much less
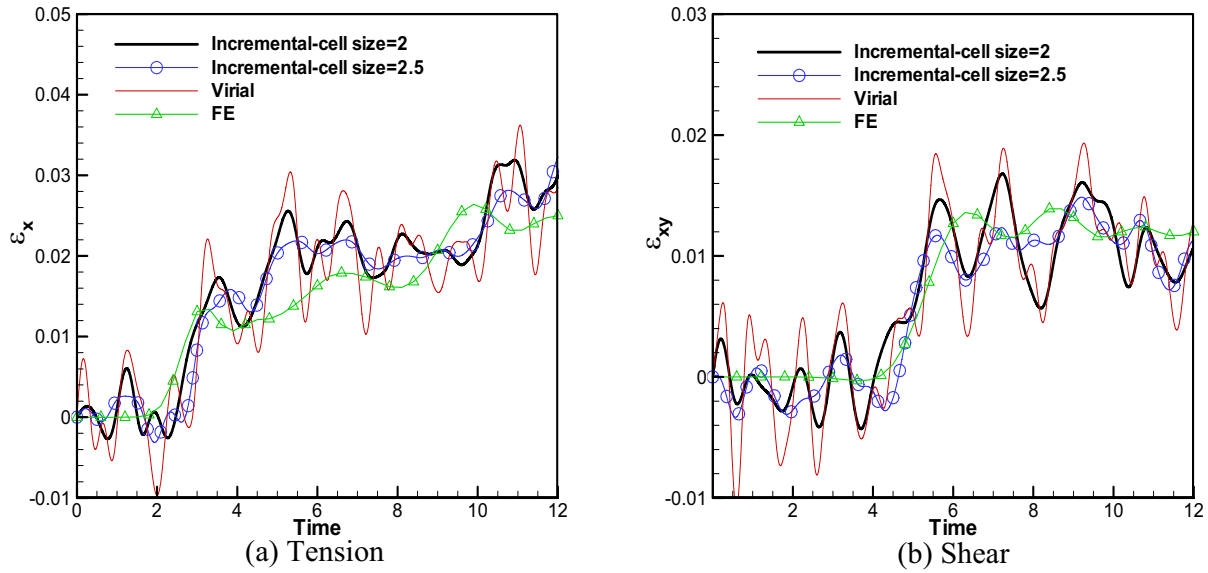
Figure 5 : Strain histories from different simulations
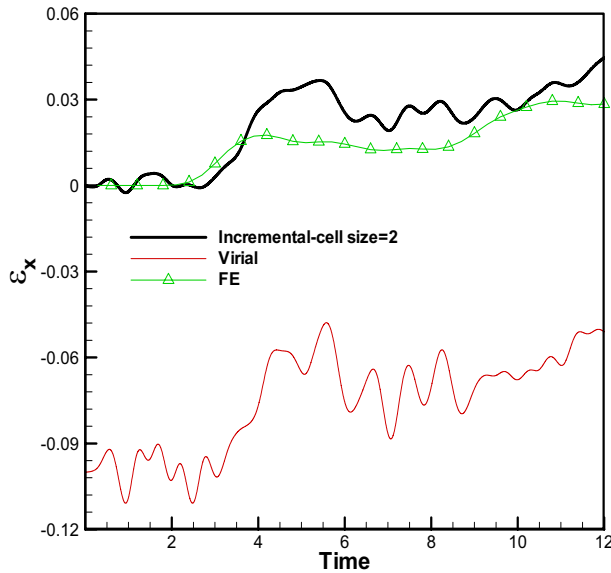
Figure 6 : Comparison of the normal strain of a surface atom in tension

oscillations.

It may be noted that the approach for the computation of the incremental atomic strain can be used for any atomic potential functions and the lattice structures, since the deformation field is evaluated at the grid nodes using interpolation. It is known that the virial formula is not applicable to atoms on the surface, see Zimmermann (1999).

The incremental formulation developed in this investigation, however, does not have this restriction because the surface velocities can be interpolated to the background grid correctly. The strains of the atom at the top surface (in the middle of the model) from three computations are plotted in Figure 6. It can be seen that atomic strain computed from the incremental strain formulation is reasonably in good agreement with the finite element analysis.

The capability to compute the strains for atoms at the boundary and at the surface is essential for coupling simulations. For example, the strain at the crack surface is needed in coupling. It may be noted that the virial formulation computes a transient strain so that it does not depend on the strain history. The incremental strain proposed herein is computed from the strain rate so that it must be computed at every time increment during the entire strain history of interest.

4 Coupling of GIMP and MD Simulations

4.1 Coupling scheme

To enable coupling between GIMP and MD, the information must be exchanged between the atomistic simulation on one side and the continuum simulation on the other. A successful coupling is indicated by the seamless transfer of the deformation, internal forces, heat, kinetic energy, etc. at the interface of two different simulation regions.

In the coupling scheme presented in this paper, heat

Incommunicado zone

(a) Overall regions of a model   (b) Transition region with background grid
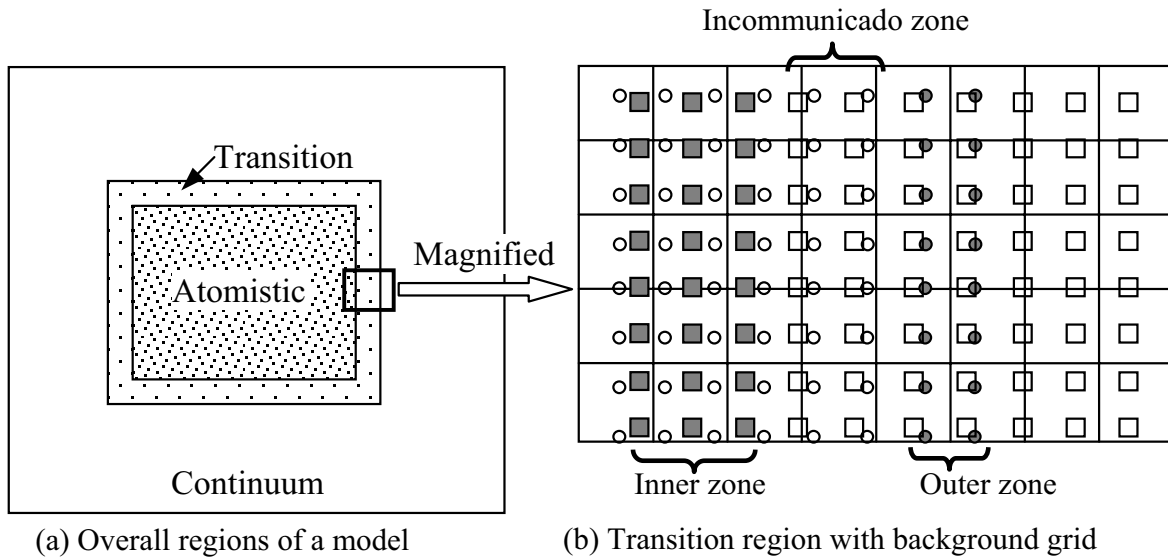
Figure 7 : Illustration of coupled GIMP and MD simulations. The circles represent atoms and squares (smaller than physical size) material points. The material points connect to each other without a gap to represent continuum

transfer between the continuum and the atomistic regions is not considered. Moreover, the transition region is assumed to remain in the linear elastic regime. Figure 7 (a) shows the overall coupling model and Figure 7 (b) shows details of the transition zone. The MD region covers a small portion of the overall model and the continuum region covers the rest. The transition region, where the communication between GIMP and MD simulations take place is divided into three zones, namely, the inner zone, the "incommunicado" zone, and the outer zone, as shown in Figure 7 (b).

In the inner zone, the information is passed from MD to GIMP. The atomic strain is computed using the incremental scheme presented in Sections 3.1 and 3.3. The velocity and strain rate at the material points overlapped within the atomistic region are computed using Eqs. (5) and (7) by replacing the atom positions with the positions of the material points. Hence, the stresses of these points are computed based on continuum theories. Consequently, the material points inside the atomistic region can be updated by the atomistic information. These material points can participate in the overall continuum computation to provide information for the rest of the continuum region. The innermost rectangle in Figure 7 (a) represents the region in which all material points are updated based on the atomistic information. These material points are shown in Figure 7 (b) as filled squares. The unfilled squares are the material points that are updated

in regular continuum computations.

The boundary atoms in the outer zone (shown as filled circles in Figure 7) update their velocities based on the interpolation of physical quantities computed at the background grid nodes using Eq. (5). The nodal velocities of the background grid are computed from the velocities of the material points weighted by the masses of the material points, as

$$V_i(t) = \frac{\sum\limits_{p} \overline{S}_{ip}(\mathrm{x}_p)\mathrm{m}_p\mathrm{v}_p(\mathrm{x}_p,t)}{\sum\limits_{p} \overline{S}_{ip}(\mathrm{x}_p)\mathrm{m}_p}. \qquad (16)$$

Once the velocities of the boundary atoms are known, their displacements can be determined from the time integration of the velocities. The width of the outer zone should be larger than the cut-off radius to ensure that the interactions with the interior atoms are fully defined by the inter-atomic potentials as in conventional MD simulations.

In the proposed coupling scheme, two different zones are used for communication in different directions, i.e. from GIMP to MD or from MD to GIMP. The "incommunicado" zone is between the inner and outer zones. This zone serves as a buffer for the communication between the material points and the atoms and contains 3 to 4 layers of material points. In this coupling scheme, iteration to obtain the converged solution in the transition zone

is not necessary, as the source of information is guaranteed to be correct and the communication in each zone is unidirectional. This approach not only simplifies the coupling algorithm but also improves the stability and reduces the computational cost.

The time step for MD simulation is usually smaller than the time step for GIMP and can be used in the coupled simulation to reach stability in coupled simulation. However, with the use of this small MD time step as the time step in the overall coupled simulation, the amount of computation is enormous. In this coupling algorithm, a temporal coupling scheme is developed. A temporal factor N is defined as the ratio of the GIMP time step to the MD time step, i.e.,

$$N = \frac{dt_{GIMP}}{dt_{MD}}, \qquad (17)$$

where $dt_{GIMP} = cL/\sqrt{E/\rho}$ is the GIMP time step, L is the cell size, and c is a constant factor (0.1 in this paper). In the coupling, MD simulation advances N time steps for each GIMP time step. In the computation, the GIMP time step is estimated first based on the ratio of the cell size to the stress wave speed. Next, the temporal factor N is rounded to an integer based on Eq. (17). Finally, the GIMP time step is determined from $dt_{GIMP} = N \cdot dt_{MD}$. The reduction in the computational time as a result of temporal coupling scheme is significant, as indicated by the numerical examples that will follow.

We next summarize the coupling scheme with the aid of the flowchart shown in Figure 8. The material points inside the atomistic domain are updated based on the nodal information interpolated from the atoms. These material points join the GIMP calculation to provide boundary conditions but are not updated again. The velocity and position of the boundary atoms are updated based on the nodal information interpolated from the material points. These boundary atoms join the MD calculation to provide the boundary conditions as well, but the velocities are not updated. The concept of temporal coupling is introduced by advancing the MD simulation N steps for every GIMP step, in order to reduce computational time. It may be noted that the material points further inside the MD region can be ignored to reduce the amount of computation since only a few layers of material points are needed to provide boundary conditions to the exterior material points.
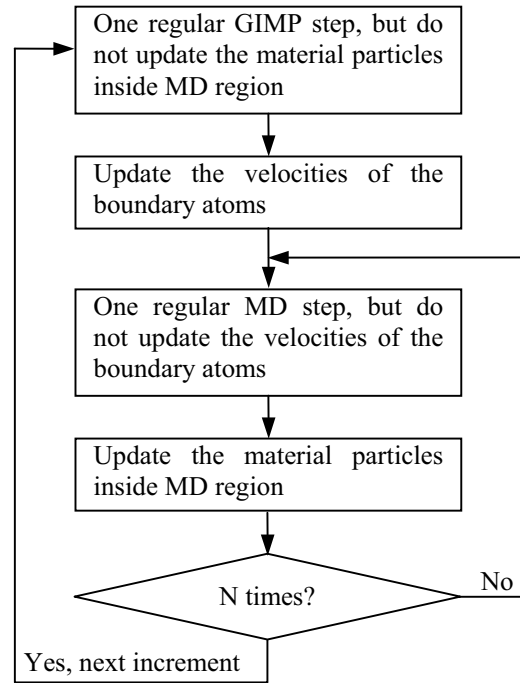

Figure 8 : Flow chart of the coupling algorithm for each increment

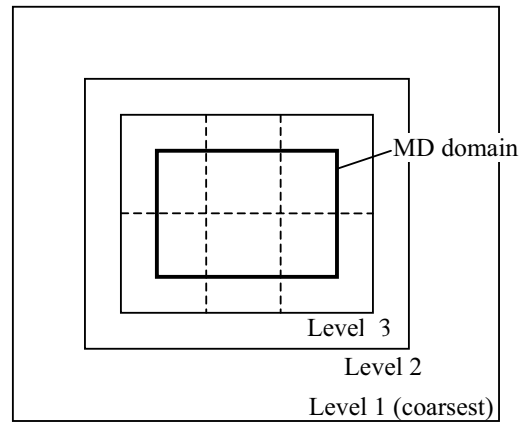### 4.2 Parallel processing of the coupled model

Figure 9 : Illustration of three GIMP grid refinements and the domain decomposition for coupling

The parallel processing for the GIMP with multilevel refinement using SAMRAI has been discussed in detail in a previous paper (Ma, Wang, Lu, Roy, Hornung, Wissink and Komanduri (2005)). The coupling between GIMP and MD is performed at the finest level only, which is always larger than the MD domain. And the finest

level is divided into rectangular regions using SAMRAI "patches". Each patch is assigned to one processor and the communication between patches is performed after each patch is computed. To eliminate data transferring between processors in the coupling process, the MD region is decomposed into rectangular regions that are of the same size as the patches. Each processor thus handles the same spatial region for both GIMP and MD. Figure 9 shows three levels of refinement for GIMP with MD coupled in the finest level. The dashed lines divide the finest level as well as the MD domain into six rectangular regions. Each region is computed by a processor and the communication between the material points and the atoms for coupling is performed within the processor. No data transfer between the processors is necessary. One disadvantage of this approach is that the load balancing of the processors is more difficult due to changing number of atoms and material points during computation.

5   Numerical Results

5.1   Multiscale simulation of mode I crack
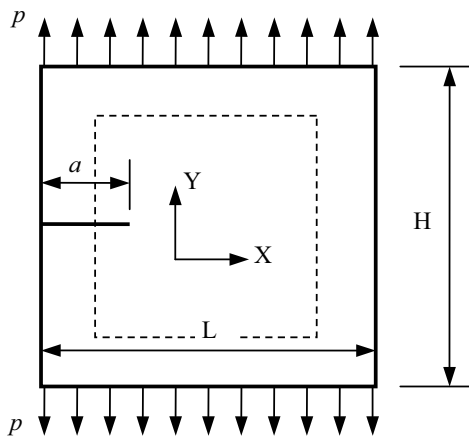
Figure 10 : Coupled GIMP/MD simulation of a 2D mode I edge crack. The dashed lines are boundaries of the atomistic domain

The coupling scheme is implemented into a multiscale simulation of a mode I crack problem as shown in Figure 10. The overall model size is 1968×1808 and the size of the MD domain is 890×600. Three levels of refinement in GIMP are applied. The finest level has a grid size of 4 and the two coarser grid sizes are 8 and 16, respectively. The finest level is coupled with MD and is divided into six patches as shown in Figure 9. It may be noted that
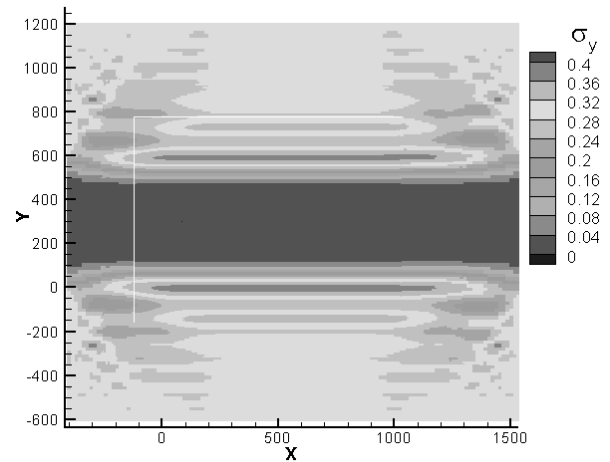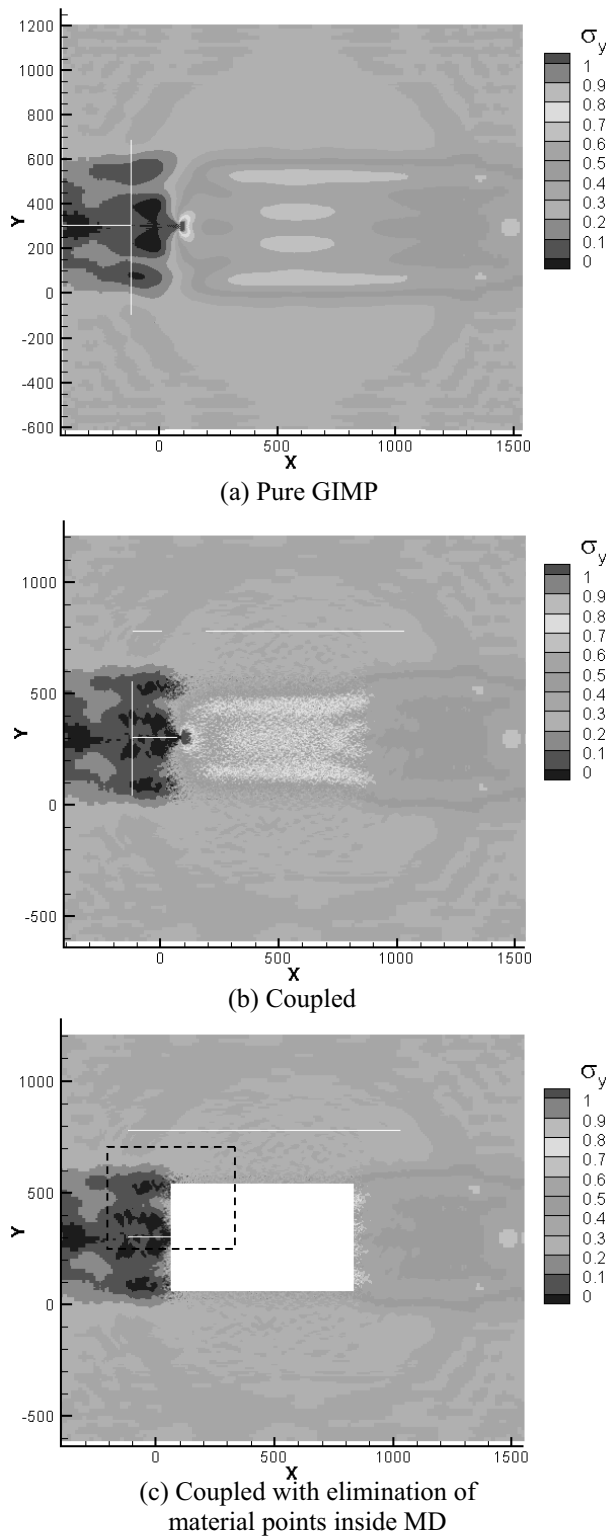

(a) Pure GIMP
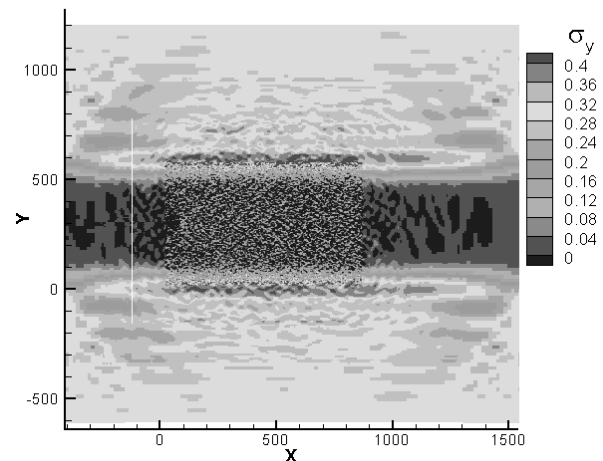
(b) Coupled
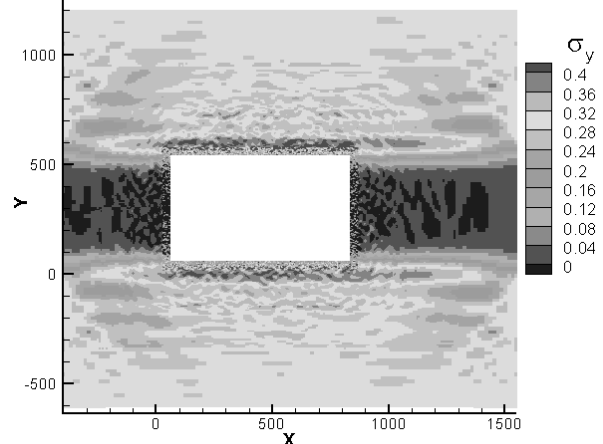
(c) Coupled after eliminating the material points inside MD

Figure 11 : Stress distribution at simulation time t = 64 with the applied pressure p = 0.3

(a) Pure GIMP

(b) Coupled

(c) Coupled with elimination of
material points inside MD

Figure 12 : Stress distribution at simulation time t = 112
with the applied pressure p = 0 .3

the sizes of the material points and the grid cells deter-
mine the cut-off wavelength that can be transmitted from
the MD simulation to the continuum. In this simulation,
the high frequency waves are not desirable in the contin-
uum region. Hence, to conserve computational time, the
minimum grid size is chosen as 4. The total number of
atoms is 497,111 and the initial crack length, *a* is 498 at
the height, Y is 301. The applied pressure, *p* is 0.3 and
the time step of the MD simulation is 0.002. The tem-
poral factor N is chosen as 40, and therefore, the GIMP
time step for the coupling level is 0.08. For comparison,
the same problem is also simulated using GIMP alone
without coupling.

Figure 11 shows the stress distribution in the model at
simulation time t = 64 when the stress wave just trav-
eled to the transition region. Figure 11 (a) corresponds
to pure GIMP simulation, and Figure 11 (b) with cou-
pling. Due to thermal vibrations of the atoms, the stress
in the MD region varies randomly between $\pm0.15\sim0.2$
at stress free state. The material points further inside the
MD region can be ignored and hence dumped to reduce
the computational load. Figure 11 (c) shows the results
for this case in which only 3 layers of material points im-
mediately inside transition region are kept and the rest
dumped. It can be seen that the stress distribution is not
affected by eliminating the material points inside the MD
region. The computational time, however, was reduced
by $\sim$50% for this case. Close to the crack tip, the stress
distribution is affected by dislocations and crack propa-
gation. In later discussions, we present only the results
with material points in the middle eliminated.

Figure 12 (a), (b) and (c) show the stress distributions
at time t = 112. At this instant the stress concentration
at the crack tip has resulted in the initiation and opening
of the crack. The stress fields from pure GIMP simula-
tion and coupled simulation are shown in Figure 12 (a)
and (b), respectively. The difference in the value of the
maximum normal stress in the Y-direction is 8%. The
coupling region is zoomed in and shown in Figure 13,
corresponding to the region indicated by the dashed rect-
angle in Figure 12 (c). The material points at three levels
of refinement are plotted with different sizes. Only 20%
of the atoms are plotted in Figure 13 to reveal the material
points within the transition region overlapped by the MD
region. The material points further inside the MD region
were eliminated in simulations as indicated in Figure 13.

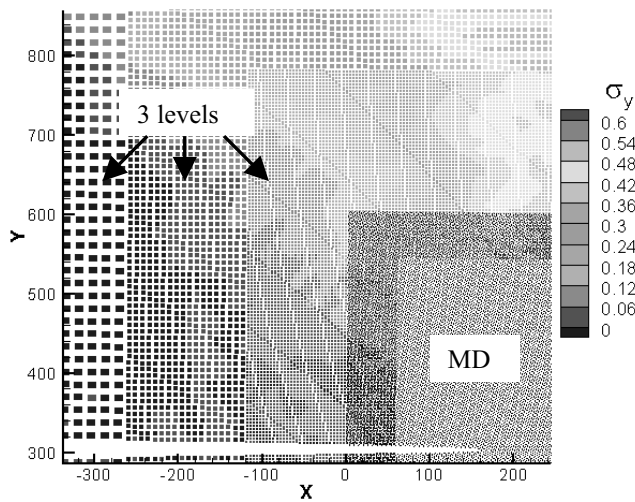It may be noted that the reduction of computational time

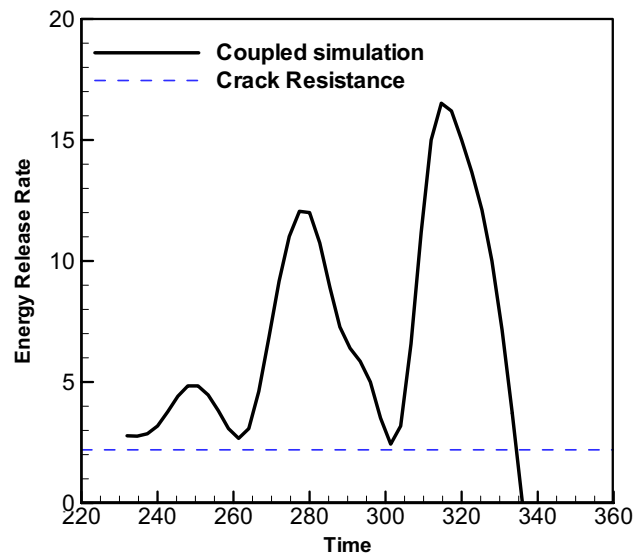**Figure 13** : Simulation model with an edge crack with p = 0.3 at t = 208

Figure 15 : Energy release rate with p = 0.15

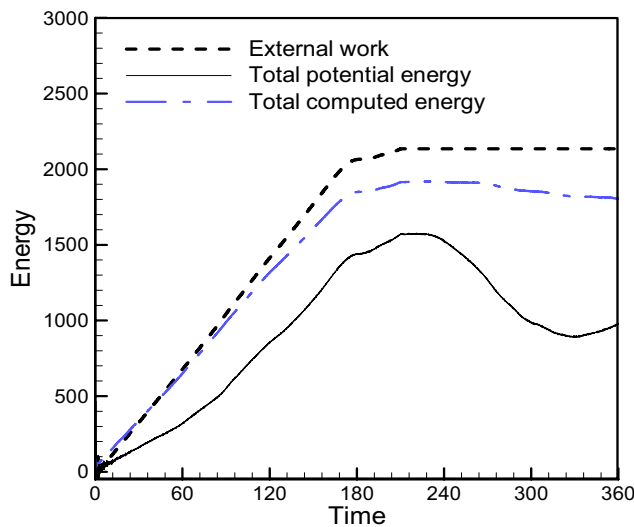**Figure 14** : Energies in the model with p = 0.15

due to temporal coupling with N = 40 is about 75% as compared to the same simulation with N = 1 (no temporal coupling). The GIMP step involves regular GIMP calculation and communication between patches and levels (refinement and coarsening). In this coupling example the computational time of one GIMP step is longer than that of an MD step. Temporal coupling has reduced the computational time significantly while maintaining the accuracy of coupling, as shown in Figure 12.

To investigate the energy release rate of a mode I crack using the coupling algorithm, a tensile pressure of 0.15 is applied from t = 0 to t = 210. The crack started to propagate at t = 225 and stopped at t = 334. The external input energy, the total potential energy and the total energy from the simulation are plotted in Figure 14. Due to numerical damping in the GIMP part of simulation, the total energy decreases as time increases. The energy loss at t = 360 is 20%. Numerical simulation was conducted for the same model without damping and the difference between the input energy and the system energy gain is less than 8%. In this case, it was observed that the total computed energy in the model varied with time about a mean value which was the external input energy. The potential energy is the sum of the potential energy of the atoms and the strain energy of the material points. It increases at first when the model is stretched. After the crack starts to propagate, the potential energy decreases. The energy release rate, as well as the crack resistance for this simulation, is plotted in Figure 15. The energy release rate fluctuates as the crack propagates and its magnitude is larger than the crack resistance. After t = 330 the energy release rate decreases below the crack resistance, leading to crack arrest.

5.2 *Atomic friction between two plates*

Next, we use the coupling algorithm to simulate the atomic friction between two plates of the same material at 0 K temperature. The model is of the same size and the MD potential is the same as the one shown in Figure
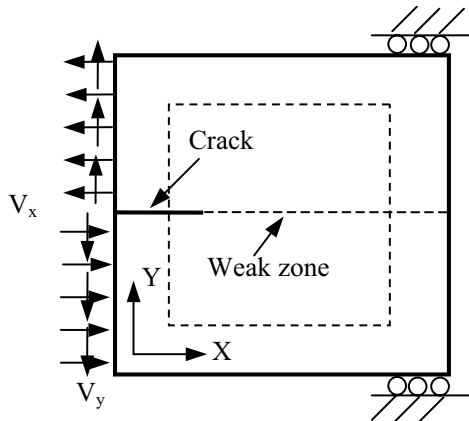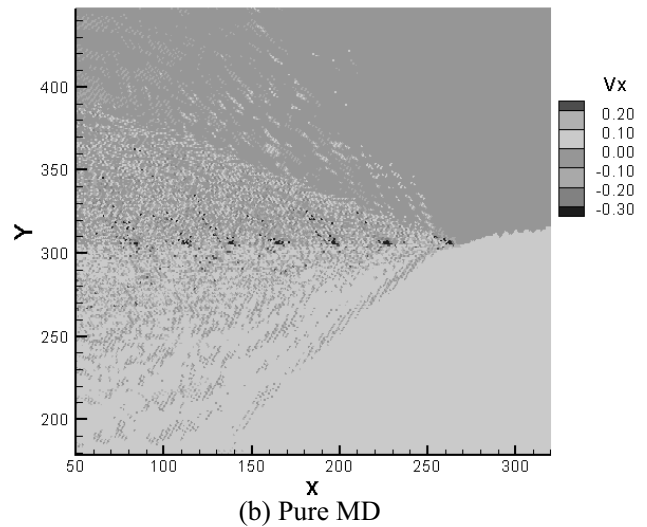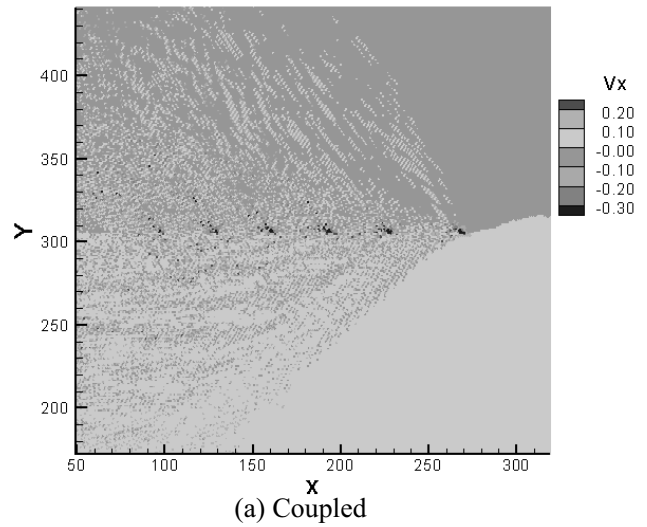
Figure 16 : Applied boundary conditions to simulate the atomic friction problem

(a) Coupled

(b) Pure MD

Figure 17 : Comparison of the velocities in the X-direction from pure MD and coupled simulations at t = 112

10. It was simulated by applying velocities on the left side of the model as shown in Figure 16. The applied shearing velocities in the X-direction, were -0.1 and 0.1 for the top and bottom halves, respectively. The interface was assumed to be atomically smooth and the friction/interaction was governed by the pairwise L-J interaction with a break radius of 1.6. Hence, the interface is a weak zone compared to the interior of each block. Moreover, in order to create a pure shearing condition at the interface and to eliminate the boundary effect, the interface up to X = 67 was set free. To avoid the contact and penetration of the free interfaces, a small velocity V_y was applied on the left boundary, 0.003 to the top half and -0.003 to the bottom half. At the right , both the top and bottom surfaces were constrained in the Y-direction to avoid possible rotation of the model in the simulation.

The velocities of the atoms in the X-direction from the coupled simulation are plotted in Figure 17 (a). The path of the shearing front was observed to be straight, as an extension to the initial free interface. The relative shearing motion between the two layers of atoms, which slipped against each other, occurred in the stick/slip mode, as indicated by Figure 17 (a). The blue spots indicate atoms moving to the left at a velocity of ∼0.7 and relative velocity between the atoms on the top and bottom is ∼0.8. Between the blue spots, the relative velocity is very small, in the range of 0 to 0.2. Most of the shear surfaces stick together and slip occurs at isolated spots.

The model was simulated with pure MD to verify the coupling algorithm. The velocities of the atoms in the X-

direction from the pure MD simulation are shown in Figure 17 (b). It can be seen that the velocity contours match well with the coupled simulations, providing further verification on the accuracy of the coupling algorithm. It may be noted that for this size of model, there are 3.3 million atoms in the pure MD simulation, and only 0.5 million atoms and three levels of material points in the coupled simulation. The computation time and memory for coupled simulation are 8% and 30% less than that for pure MD simulation, respectively. As the model grows bigger, there will be more savings in both computation time and memory consumption.

As shown in Figures 18 (a) and (b), at t = 56, the first
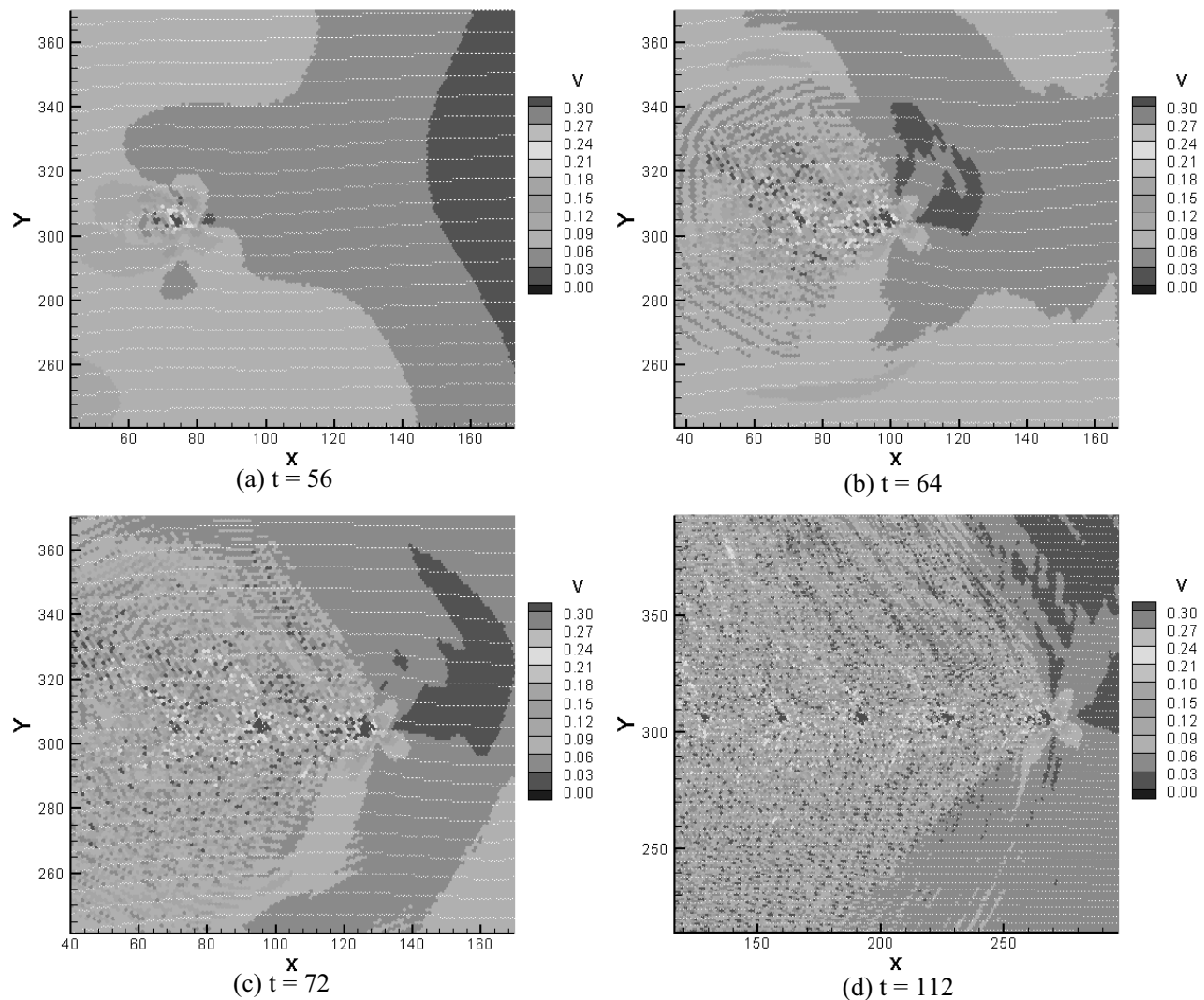
Figure 18 : Evolution of multiple slip and Mach lines

slip spot is generated at the crack tip and it propagates to the right at a speed of 3.2. At t = 64, a second slip is developed, respectively. At t = 72, a third slip is developed and symmetric Mach lines at the first slip location can be observed clearly and these Mach lines form a 45 degree angle with the slip path as shown in Figure 18 (c). The Mach lines travels in the same direction as the slip location and a pair of Mach lines are generated for each subsequent slip location. The Mach lines for different slip locations are nearly parallel to each other, as shown in Figure 18 (d). Similar Mach lines under micro stick/slip conditions were observed by Coker, Lykotrafitis, Needleman and Rosakis (2005) at the continuum scale.

The atom velocities and potential energies along the slip

plane at t = 112 are plotted in Figure 19. The deep valleys in the velocity diagram correspond to the slip zones, slipping to the left as indicated by negative velocities. The areas of small variation in velocity between neighboring deep valleys correspond to the stick area. Within the stick zone between two deep valleys in velocity diagram, the oscillation in velocity could potentially indicate some stick/slip at a smaller scale within the larger scale stick zone. It may be noted that a zero Kelvin temperature was assigned at the beginning of the simulation, so that the velocity variation between two deep valleys was most likely induced by even smaller scale stick/slip phenomenon.

The potential energy at each slip zone is high due to
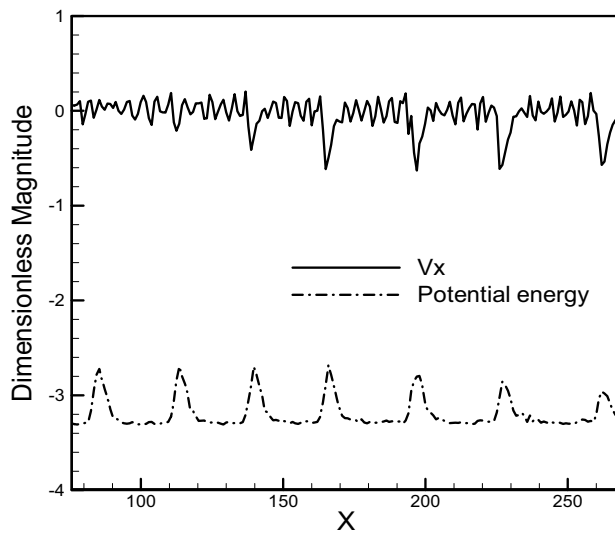
Figure 19 : Atom velocity and potential energy along slip plane at t = 112

lattice dislocations along the slip plane. Within each stick zone, the potential energy is low, indicating that the atoms have partially returned to the regular lattice positions, giving lower potential energy as a result. This process is usually called self-healing. It can be seen from Figure 19 that both kinetic (inferred from velocity diagram) and the potential energies at each slip zone are high. During slipping, the atoms on top of the slip plane move to the left according to the applied boundary condition, pulling the neighboring atoms at the right to the left, and transferring part of the high energies to these neighboring atoms at the right, and in the meanwhile, causing the slip pulse to move to the right. As the shearing continues, slip zones possessing high energies are created one by one and extend to the right.

6   Conclusions

A coupled atomistic/continuum simulation method is presented by coupling MD simulations with GIMP simulations. To enable coupling, a method for the computation of atomistic strain is developed based on the computation of strain rate. The atomic strain rate is computed by first interpolating the velocities of the atoms to the background Eulerian grid and then computing the gradient of grid velocities. The computed atomic strain shows less cyclic variation than that computed by the virial theorem due to noise reduction in the interpolation process.

The generalized interpolation function is chosen as the interpolation function for GIMP and a structured grid is used for the background grid. The atomic stress is then computed based on strain using the isotropic and homogeneous constitutive law.

The coupling algorithm uses a common background grid for MD and GIMP. The velocities of the boundary atoms are computed from the grid velocities which are interpolated from the material points. The material points inside the MD region are updated based on the atomic information and these points join rest of the material points in the GIMP computation. This approach ensures the compatibility of deformation and stresses at the MD/GIMP interface region.

A multi-level refinement scheme for GIMP is used to refine the material points close to the atomistic size. The coupling algorithm is implemented using the SAMRAI (Structural Adaptive Mesh Refinement Application Infrastructure) for parallel processing. The finest GIMP level is coupled with the MD simulation. The MD region is decomposed into domains with the same geometry as the GIMP patches. Each patch is assigned to a processor and the coupling between the atoms and material points is performed inside each processor without extra interprocessor communication.

The coupling algorithm was verified by comparing the coupling results with pure GIMP and pure MD simulations.

A mode I crack propagation problem was simulated using the coupling technique presented here. The stress field of the coupled model is verified through comparison with pure GIMP simulations in the elastic stage. The energy release rate is also computed. It is found that the crack arrests after the energy release rate is less than the crack resistance.

In model II loading, stick/slip pulses were observed at the crack surfaces and the results compared well with pure MD simulation. Within (larger) the sticking zones there are smaller scale high frequency component of stick/slip pulses.

While the current implementation is in 2D, the coupling algorithm can be extended to 3D.

References

Allen, M.P.; Tildesley, D.J. (1989): *Computer Simulation of Liquids*, Oxford University Press.

Bardenhagen, S.G; Kober, E.M. (2004): The generalized interpolation material point method. *CMES: Computer Modeling in Engineering & Sciences*, v5 n6, pp. 477-496.

Buehler, M.J.; Abraham, F.F.; Gao, H. (2003): Hyperelasticity governs dynamic fracture at a critical length scale. *Nature*, v426, pp. 141-146.

Buehler, M.J.; Gao H.; Huang, Y. (2004): Atomistic and continuum studies of stress and strain fields near a rapidly propagating crack in a harmonic lattice. *Theoretical and Applied Fracture Mechanics,* v41, pp.21-42.

Cai, W.; Koning, M.; Bulatov, V.; Yip, S. (2000): Minimizing boundary reflections in coupled-domain simulations. *Physical Review Letters*, v85 n15, pp. 3213-3216.

Coker, D.; Lykotrafitis; Needleman, A. and Rosakis, A.J. (2005): Frictional sliding modes along an interface between identical elastic plates subject to shear impact loading. *Journal of the Mechanics and Physics of Solids*, v53, pp. 884-922

Curtin, W.A.; Miller, R.E. (2003): Atomistic/continuum coupling in computational materials science. *Modeling and Simulation in Materials Science and Engineering*, v11, R33-R68.

Gao, H.; Huang, Y.; Abraham, F.F. (2001): Continuum and atomistic studies of intersonic crack propagation. *Journal of the Mechanics and Physics of Solids*, v49, pp. 2113-2132.

Guo, Y.; Nairn, J.A. (2004): Calculation of J-integral and stress intensity factors using the material point method. *CMES: Computer Modeling in Engineering & Sciences*, v6 n3, pp.295-308.

Hardy, R.J.; Root, S.; Swanson, D.R. (2002): Continuum properties from molecular simulations. *AIP Conference Proceedings*, n620 pt1, pp 363–366.

Hornung, R.D.; Kohn, S.R. (2002): Managing application complexity in the SAMRAI object-oriented framework. *Concurrency and Computation: Practice and Experience*, v14, pp. 347-368.

Horstemeyer, M.F.; Baskes, M.I. (2000): Strain tensors at the atomistic scale. *Materials Research Society Symposium Proceedings*, v578, pp.15-20.

Kohlhoff, S.; Gumbsch, P.; and Fischmeister, H.F. (1991): Crack propagation in b.c.c. crystals studied with a combined finite-elment and atomistic model. *Philosophical Magazine, A*, v64 n4, pp.851-878.

Ma, J., Wang, B., Lu, H., Roy, S., Hornung, R., Wissink, A. and Komanduri, R. (2005): Multiscale simulations using generalized interpolation material point method (GIMP) and SAMRAI parallel processing. *CMES: Computer Modeling in Engineering & Sciences*, v8 n2, pp. 135-152.

Marc, G. and McMillan, W.G. (1985): The virial theorem. *Advances in Chemical Physics*, v58, pp.209-361.

Plimpton, S.J. (1995): Fast Parallel Algorithms for Short-Range Molecular Dynamics. *Journal of Computational Physics*, v117 n1, pp. 1-19.

Rafii-Tabar, H., Hua, L. and Cross, L. (1998): A multiscale atomistic-continuum modeling of crack propagation in a two-dimensional macroscopic plate. *Journal of Physics: Condensed Matter*, v10, pp. 2375-2387.

Rudd, R. E. and Broughton, J.Q. (1998): Coarse-grained molecular dynamics and the atomic limit of finite elements. *Physical Review B*, v58 n10, pp. R5893-5896.

Shen, S. and Atluri, S.N. (2005): A tangent stiffness MLPG method for atom/continuum multiscale simulation. *CMES: Computer Modeling in Engineering & Sciences*, v7, n1, pp. 49-67.

Shiari, B., Miller, R.E. and Curtin, W.A. (2005): Coupled atomistic/discrete dislocation simulations of nanoindentation at finite temperature. *Journal of Engineering Materials and Technology*, v127, pp.358-368.

Shilkrot, L.E., Miller, R.E. and Curtin, W.A. (2002): Coupled atomistic and discrete dislocation plasticity. *Physical Review Letters*, v89 n2, 025501.

Sulsky, D. and Schreyer, H.L. (1996): Axisymmetric form of the material point method with applications to upsetting and Taylor impact problems. *Computer Methods in Applied Mechanics and Engineering*, v139, pp.

409-429.

Sulsky, D., Zhou, S.J. and Schreyer, H.L. (1995): Application of a particle-in-cell method to solid mechanics. *Computer Physics Communications*, v87 n1-2, pp. 236-252.

Zhou, M. and McDowell, D.L. (2002): Equivalent continuum for dynamically deforming atomistic particle systems. *Philosophical Magazine, A*, v82 n13, pp.2547-2574.

Zimmermann, J.A. (1999): Continuum and atomistic modeling of dislocation nucleation at crystal surface ledges. *Ph.D. dissertation*, Stanford University.

Zimmermann, J.A., Webb III, E.B., Hoyt, J.J., Jones, R.E. Klein, P.A. and Bammann, D.J. (2004): Calculation of stress in atomistic simulation. *Modeling and Simulation in Materials Science and Engineering*, v12, S319-S332.